Risk assessment of urban infrastructure vulnerability to meteorological disasters: A case study of Dongguan, China

Fan Li [a,b], Yan Li [c], Matteo Rubinato [d,*], Yu Zheng [a,b], Tao Zhou [e]

[a] *School of Environment and Civil Engineering, Dongguan University of Technology, Dongguan, 523808, China*

[b] *Guangdong Provincial Key Laboratory of Intelligent Disaster Prevention and Emergency Technologies for Urban Lifeline Engineering, Dongguan University of Technology, Dongguan, 523808, China*

[c] *School of Civil and Transportation Engineering, Guangdong University of Technology, Guangzhou, 510000, China*

[d] *Department of Civil Engineering, College of Engineering and Physical Sciences, Aston University, Birmingham, B4 7ET, UK*

[e] *School of Management Science and Real Estate, Chongqing University, Chongqing, 400044, China*

A B S T R A C T

Effective forecasting and response to meteorological hazards are crucial for safeguarding life, property, and supporting sustainable socioeconomic development. With the rising frequency and severity of meteorological hazards worldwide, this study proposes an enhanced risk assessment framework for urban infrastructure exposed to extreme weather events, with a focus on cascading impacts to critical services such as electricity, communication, and transportation networks (roads and subways). A disaster-loss model is developed to quantify infrastructure vulnerability at various spatial and temporal scales under heavy rainfall conditions, accounting for secondary effects. The model's performance is validated through empirical analysis of a 15-year rainfall event in Dongguan City, China, occurring from September 7–8, 2023. Results indicate the model's ability to predict real-event outcomes with approximately 70% accuracy. This model offers valuable insights for disaster prevention and mitigation strategies, aiding decision-makers in optimizing emergency resource allocation, enhancing disaster response efficiency, and issuing timely public risk warnings to minimize losses.

1. Introduction

Over the past two decades, China has experienced numerous meteorological hazards [1,2], predominantly triggered by heavy storms, including tropical storms, extra-tropical cyclones, and local convective storms. These meteorological hazards account for over 70% of all recorded hazards (Geophysical, Hydrological, Climatological, Biological, and Extra-terrestrial) [3]. Among these, heavy rainfall is the primary contributor to losses associated with meteorological hazards [4]. For instance, heavy rainfall often leads to secondary hazards such as flooding, waterlogging, landslides, power outages, and communication failures, all of which pose significant risks to human safety and property [5].

While hazards like heavy rainfall and floods are natural phenomena, their transformation into disasters is often a consequence of human activities and policy decisions [6–9]. Rapid urbanization and industrialization have increased the urban population, complicating the ability of existing measures to mitigate meteorological hazards. This has particularly affected emergency response

---

* Corresponding author.
E-mail address: m.rubinato@aston.ac.uk (M. Rubinato).

capabilities, given the sensitivity and variability of disaster-prone environments, increased exposure of vulnerable populations, and the complexity of disaster-inducing factors [10]. The growing interconnectedness of global systems has exacerbated the derivative, in-direct impacts, and cascading effects of hazards, presenting significant challenges to sustainable development [11–13]. Consequently, traditional single-hazard, single-timepoint, and broadly generalized risk assessment models are increasingly insufficient for addressing the multi-hazard, long-duration, and finely-tuned disaster prevention scenarios required today.

Most prior research on disaster chains or cascading infrastructure failures has been conducted at the macro-system level [14–16]. These studies typically construct indicator systems to assess the integrated risk levels of infrastructure in a given area [17,18] or focus on the resilience and vulnerability of urban infrastructures to external shocks [19–21]. However, such studies often overlook the spatial dimension and fail to conduct detailed risk assessments for specific infrastructure nodes.

Conversely, most micro-level studies on infrastructure risk provide fine-grained assessments by dividing the study area into small grids to analyze integrated risks within grid boundaries [14,22] or examine the risk levels of specific infrastructure nodes under the impact of a single hazard type [23–28]. However, these micro-level studies often neglect the effects of secondary hazards triggered by emergencies.

To address these gaps, this paper explores the rainstorm disaster chain and the mechanisms of cascading failures within infra-structure nodes. Based on this analysis, we propose a novel theoretical model for assessing the failure risk of urban infrastructure under the influence of rainstorms and their secondary hazards. The validity and effectiveness of the model are tested using a real-world scenario. Theoretically, this study focuses on the impacts of rainstorm-induced disaster chains on urban infrastructure, contributing to the existing body of knowledge on risk assessment for single-hazard scenarios. Additionally, the study advances the theory of refined risk assessment by examining the risk levels of urban infrastructure in both spatial and temporal dimensions, thus enriching the broader framework of macroscopic risk assessment.

From a practical standpoint, this study (i) develops a disaster-loss calculation model based on rainstorm disaster chains and cascading failure mechanisms within infrastructure nodes, (ii) predicts the evolution of disaster risk from a spatio-temporal perspective, and (iii) provides targeted disaster risk predictions for specific infrastructure nodes at different times and locations. This model offers significant practical value for improving the layout of emergency response strategies, enhancing the precision of resource allocation, and enabling dynamic decision-making in multi-hazard emergency situations.

2. State-of-the-art

Existing studies on disaster chains and cascading infrastructure failures have predominantly been conducted at the macro-system level [29–31]. These studies can be broadly classified into four main categories. First, many focus on constructing socioeconomic indicator systems related to hazard response or resilience to assess the overall resilience of infrastructure within the study area [17,18]. Second, some studies aim to establish correlation networks between disaster-causing factors and infrastructure damage events based on historical disaster cases. These studies use complex network models or Bayesian networks to identify key events or critical links influencing infrastructure risk [19,20,32,33]. Third, a number of studies examine the correlation between multiple infrastructure systems (e.g., water, electricity, natural gas, communication, and transportation) to assess the effects of localized failures, external resources, system delays, and interventions on systemic infrastructure risk [21,23,34,35]. Finally, some studies focus on developing quantitative models for the transmission of disaster risks across infrastructure systems, evaluating their resilience and vulnerability after hazard shocks [36,37].

However, most of these studies concentrate on the overall resilience or vulnerability of infrastructure systems, often neglecting the specific risks faced by individual infrastructure nodes. Such node-specific, time-sensitive risk assessments are crucial for guiding refined disaster prevention strategies.

Several studies have considered the spatial location of infrastructure in micro-level risk assessments. For example, Singh et al. [38] assessed the vulnerability of urban road networks after flooding using hydrodynamic simulations and velocity function statistics, identifying the spatial distribution of heavily inundated and dysfunctional road networks. However, they focused solely on the impact of flooding on a single type of infrastructure [38]. Hsu et al. [22] divided the study area into 500m × 500m grids, calculating the combined vulnerability of water, electricity, and transportation infrastructure within each grid to assess regional risk following an earthquake. However, this study overlooked cascading failures between infrastructure systems, instead simplifying the risk as a su-perposition of individual systems' vulnerabilities [22]. Bao et al. [39] employed dynamic cascading analysis and Monte Carlo sim-ulations to construct a correlation network between power and natural gas infrastructure nodes, assessing their reliability after external disturbances. This approach, however, treated the initial failure of infrastructure nodes as random events and did not adequately quantify the risks posed by external shocks [39]. Similarly, Loggins and Wallace [40] used Monte Carlo simulations to model the damage to infrastructure nodes, such as power, water, and communications, following a hurricane, but focused primarily on a single hazard, ignoring its secondary effects [40].

These previous studies provide important references for understanding cascading failure mechanisms and disaster-damage models in urban infrastructure. However, most micro-level studies focus on single emergencies and overlook the secondary hazards that can be triggered by primary events. As urbanization increases, the complexity of disaster-causing factors, disaster-prone environments, and vulnerable populations has also grown. This makes the accurate quantification of secondary effects—triggered by primary hazard-s—both more challenging and more crucial. The objective of this study is to address this gap by examining the impacts of multiple hazards on infrastructure nodes and the associated chain effects.

Furthermore, numerous studies in disaster management emphasize the importance of pre-disaster prevention, preparation, and planning, which rely heavily on the results of refined pre-disaster risk assessments [41–43]. This study contributes to this need by

conducting a refined risk assessment of infrastructure under the influence of multiple hazards, offering predictive insights into potential risks before they occur. This approach is essential for mitigating the exposure and vulnerability of people, property, and infrastructure.

The methodology employed in this study follows four main steps: i) constructing the rainstorm disaster chain, specifying the types of secondary hazards triggered by rainstorms; ii) analyzing the cascading failures within infrastructure systems; iii) developing a disaster-loss model to evaluate the risk levels of secondary hazards and their impact on infrastructure nodes, comparing these risk levels against threshold values to determine the operational status (normal or failed) of each infrastructure node; iv) analyzing the spatial distribution of failed infrastructure nodes due to cascading failures at multiple time points. This process is implemented programmatically using Python software to simulate and assess infrastructure risks under the influence of multiple hazards.

This study distinguishes itself from prior research through several key innovations: it focuses on the impact of multiple hazards on infrastructure, specifically heavy rainfall and its secondary hazards, rather than a single hazard type. It emphasizes refined risk assessment rather than a generalized assessment of the overall infrastructure network. The refined assessment is reflected in two dimensions:

- First, it provides time- and location-specific risk assessments of infrastructure nodes in both spatial and temporal dimensions.
- Second, the study area is divided into fine grids to calculate multi-hazard risks within each grid, assessing the initial failure nodes caused by hazards before analyzing the cascading failure propagation from these nodes. This approach contrasts with methods that set random initial failure nodes and focus solely on cascading failures between nodes.

The findings of this study provide a critical reference for developing refined disaster prevention strategies under multi-hazard scenarios.

3. Methods

3.1. Refined risk assessment for infrastructure

The refined risk assessment aims to evaluate the risk levels for individual infrastructure nodes under the influence of the rainstorm
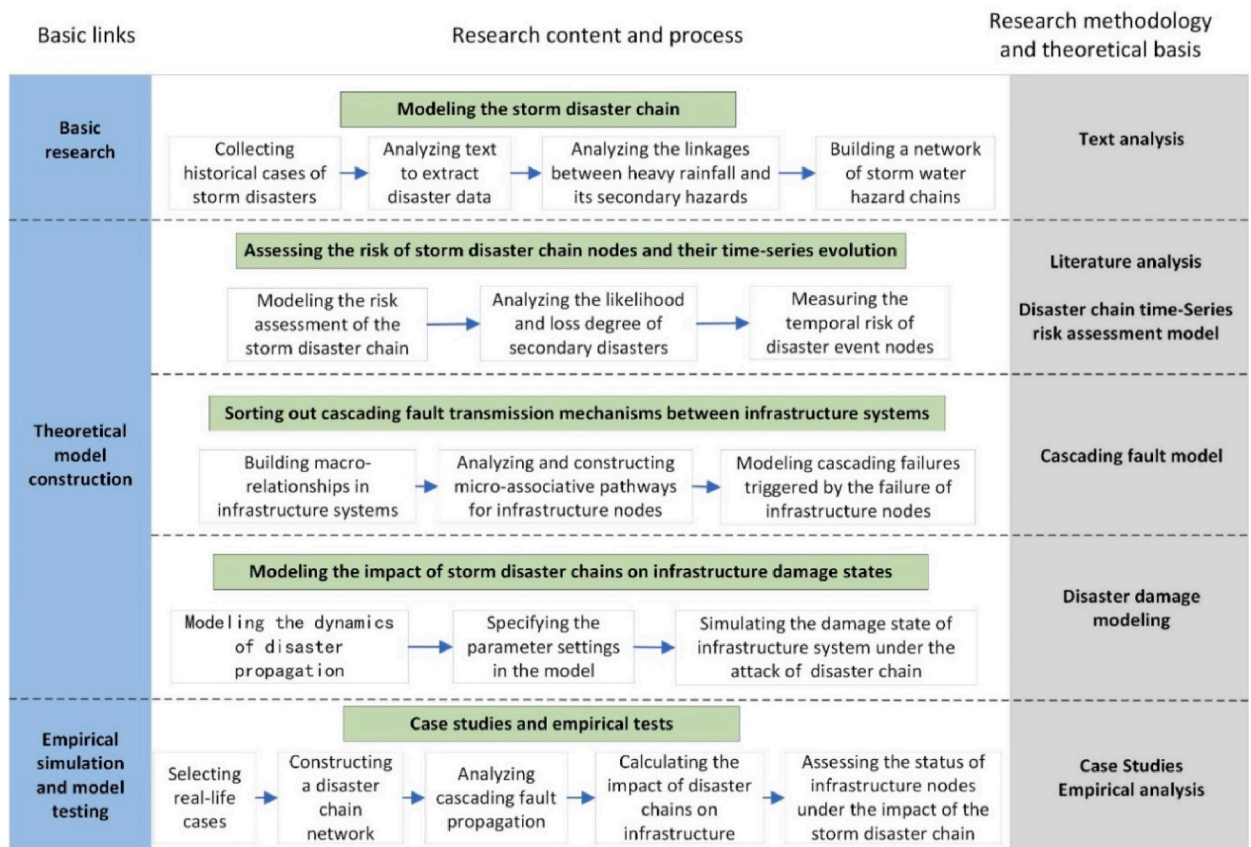

Fig. 1. Overview of the refined risk assessment framework for infrastructure.

disaster chain at specific times and locations. The infrastructures considered in this study include power supply systems, electric power communication systems, subway transportation systems, and road transportation systems, referred to here as power, communication, subway, and road, respectively.

To achieve this objective, the first step involved constructing the rainstorm disaster chain for the study area. Following this, an infrastructure correlation network was developed based on the cascade fault transmission mechanism within and between infrastructure systems. Finally, a disaster-damage model was created, incorporating both the rainstorm disaster chain and the cascading failure impacts on each infrastructure type. The schematic diagram illustrating the overall conceptual framework of this study is presented in Fig. 1.

3.2. Construction of the rainstorm disaster chain

A disaster chain refers to the phenomenon where one disaster triggers a series of subsequent disasters [44]. The core components of a disaster chain include disaster-causing factors, the disaster-conceiving environment, and the disaster-bearing body. The occurrence of a disaster results from the complex spatiotemporal coupling of these core elements [45]. Within the disaster chain, disasters exhibit deep mutual interdependence and strong interactions, constantly exchanging material, energy, and information with their surrounding environment. This forms a complex, dynamic feedback system [46].

In constructing the urban rainstorm disaster chain, it is essential to gather a wide range of data related to rainstorm events, including news reports, disaster documentation, and government records. The collected data, whether from the main rainstorm event or secondary disasters potentially triggered by it, are then analyzed to identify possible linkages. Finally, these correlations are examined to establish the disaster evolution chain or network, based on direct or indirect relationships between the events and the rainstorm disaster.

3.3. Analysis of cascading faults within infrastructure

Cascading effects in infrastructure systems are highly complex, involving dynamic interdependencies. Cascade failure analysis investigates the chain reactions triggered within infrastructure systems when one or more points of failure occur [47]. When a component or node within an infrastructure system fails, this failure can propagate rapidly throughout the system and may trigger broader chain reactions across interconnected systems. These reactions often span multiple physical, social, and economic dimensions, leading to damage that far exceeds the initial failure [48]. Understanding and analyzing these cascading effects are critical to preventing and mitigating potential disaster risks, thereby ensuring system stability and safety.

Urban infrastructure systems typically include water supply, electric power, communication, natural gas, and transportation networks. Due to data availability, this study focuses on power, communication, subway, and road systems. When a part of these systems fails due to a shock induced by a hazard, other connected infrastructure nodes may also be at risk, both within the same system and across different systems. The interdependencies among infrastructure systems are often identified through empirical analysis.

Fig. 2 illustrates the relationships between infrastructure systems following a rainstorm event. Notably, there is an interdependent relationship between the power and communication systems. The power system relies on the communication system for transmitting operational commands and data for system control, while the communication system depends on the power system for a stable electricity supply. Furthermore, the subway system depends on the power system for normal operations, and disruptions in the road system could affect accessibility to subway stations.
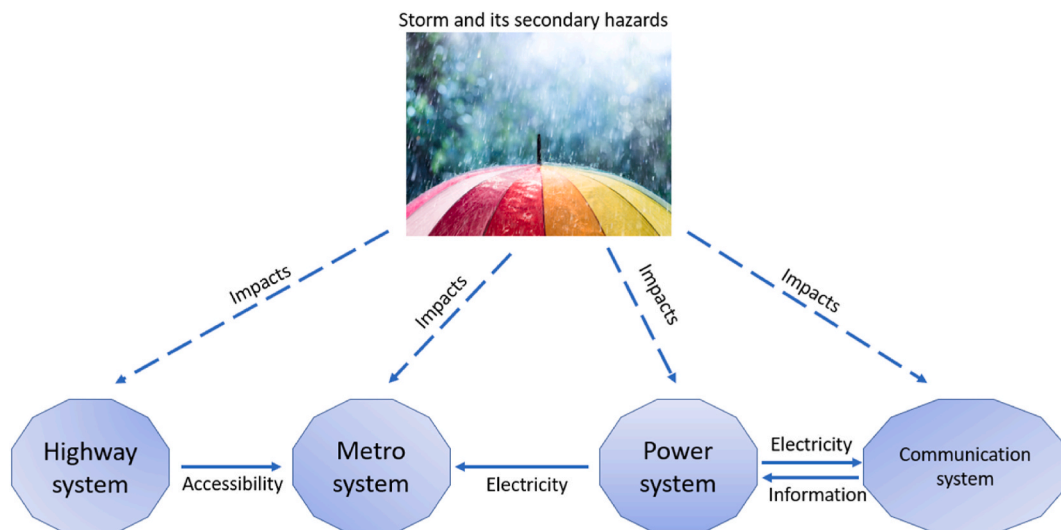

Fig. 2. Relationships between infrastructure systems following a rainstorm hazard.

To develop a fine-grained disaster prevention strategy, it is essential to conduct a timely and location-specific assessment of infrastructure risk. In addition to understanding the macroscopic correlations between different infrastructure systems, it is equally important to analyze the cascading failure transmission mechanisms between specific infrastructure nodes at the micro level. Significant cascading failure interactions include the interdependence between power and communication systems, the direct impact of power on metro systems, and the influence of road systems on metro operations. The micro-level analysis of these cascading failures provides a detailed schematic of the correlation network between infrastructure nodes, as illustrated in Fig. 3.

In Fig. 3, the associations between nodes in each infrastructure layer are constructed based on real-life connections. For instance, subway stations are linked according to the layout of subway lines, while the midpoints of road segments are connected according to the configuration of the roads. In China, roads are categorized into national highways, provincial highways, county highways, and township roads based on administrative divisions. Additionally, they can be classified into expressways, primary roads, secondary roads, tertiary roads, and quaternary roads according to their status and technical specifications. The road types included in the road network for this study primarily encompass national highways, provincial highways, county highways, primary roads, secondary roads, tertiary roads, and quaternary roads. These seven categories are integrated to create a road network layer using ArcGIS software. Since expressways and township roads are typically absent within several hundred meters of a subway station, these two categories are excluded from the analysis.

In the electric power layer, a network is established based on the actual associations between power plants, substations, and charging stations. For example, substations are connected to power plants to receive electricity, while charging stations are linked to substations for low-voltage power supply. In the communication system, each communication site may provide information and communication services for the power system. Communication stations are interconnected based on their functional collaborations, with the power information dispatch center being the most closely linked to the other stations.

In addition to examining the correlations among infrastructure nodes within the same layer, it is also crucial to analyze the cascading failures between infrastructure nodes across different layers. The specific analysis can be structured as follows.

3.3.1. Power and communication systems

Fig. 4 illustrates the micro-analytic diagram of cascading fault propagation for power and communication nodes. This diagram draws on previous literature [49,50] to simulate the propagation process of cascading faults between networks through a simplified model, without accounting for the complex dynamics present in actual transmission and distribution networks. There exists an interdependence between power and communication nodes; when a disaster-induced shock results in a failure of a communication node, this failure is transmitted to the associated power node. Conversely, when a power node experiences a failure due to a disaster shock, this failure will be relayed to the connected communication node.

Specifically, within the communication network, when node C0 fails as a result of a hazard, it triggers the propagation of a cascading fault. In the subsequent phase, the electricity node E0, which depends on C0, along with the edges connecting C0 and E0, is simultaneously removed. In the second phase, neighboring nodes within the network may fail due to load overruns; thus, edges connecting other electricity nodes (e.g., E1 and E2) to isolated communication nodes are also removed. The third stage involves similar processing of the communication network nodes, culminating in the formation of the final network state.
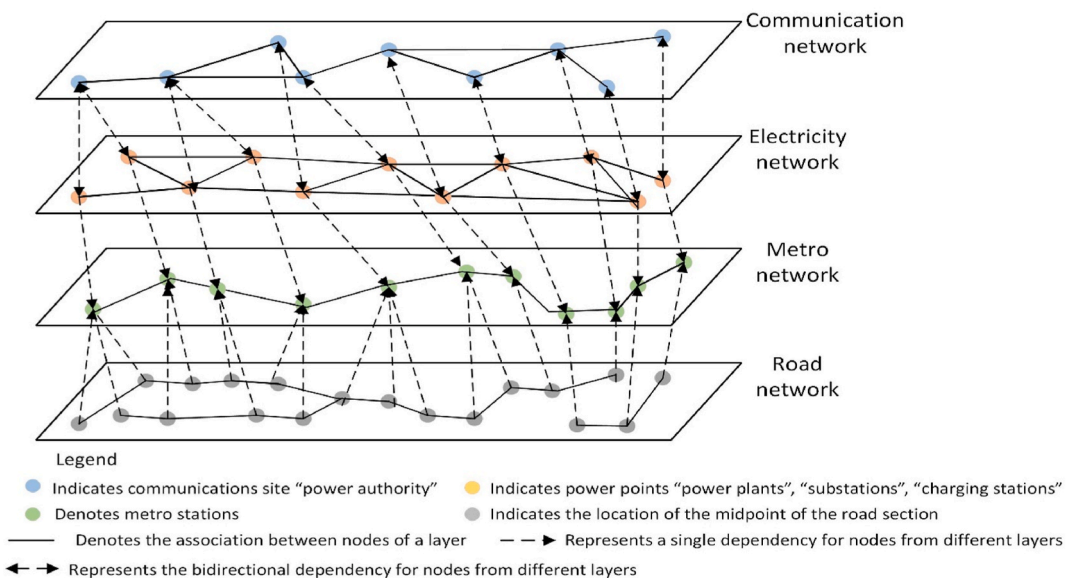

Fig. 3. Schematic diagram of infrastructure node association network synthesis.
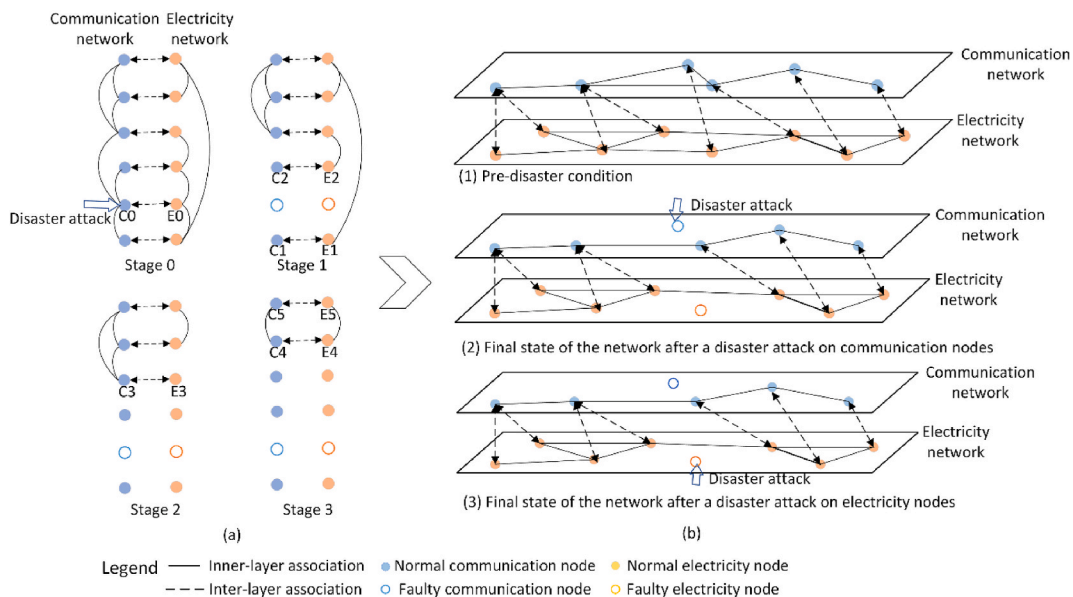
Fig. 4. The iterative process (a) and results (b) of cascading faults for communication and power nodes.

3.3.2. Power and subway systems

Fig. 5 illustrates the micro-analysis of cascading faults between power and metro nodes. There exists a single dependency between power and metro systems, as the normal operation of metro nodes relies on the power supplied by power nodes. Therefore, when a power node (E0) fails due to a disaster shock, it results in the failure of the linked metro node (M0), and the edges connecting nodes E0 and M0 are removed synchronously. Conversely, when a metro node (M0) fails due to a disaster shock, only the edges of the metro network connected to it are removed; this failure does not propagate to affect the power node.

3.3.3. Subway and road systems

In the context of the rainstorm disaster chain, there exists a unidirectional impact relationship between subway and road systems. Fig. 6 presents the micro-analysis diagram of cascading failures between subway and road nodes. When the nodes of road traffic sections (R0) within a certain range of a subway node (M0) fail, the normal access for passenger flow to that subway station may be disrupted, resulting in a failure of the subway station's function, along with the removal of the edges connected to R0 and M0.
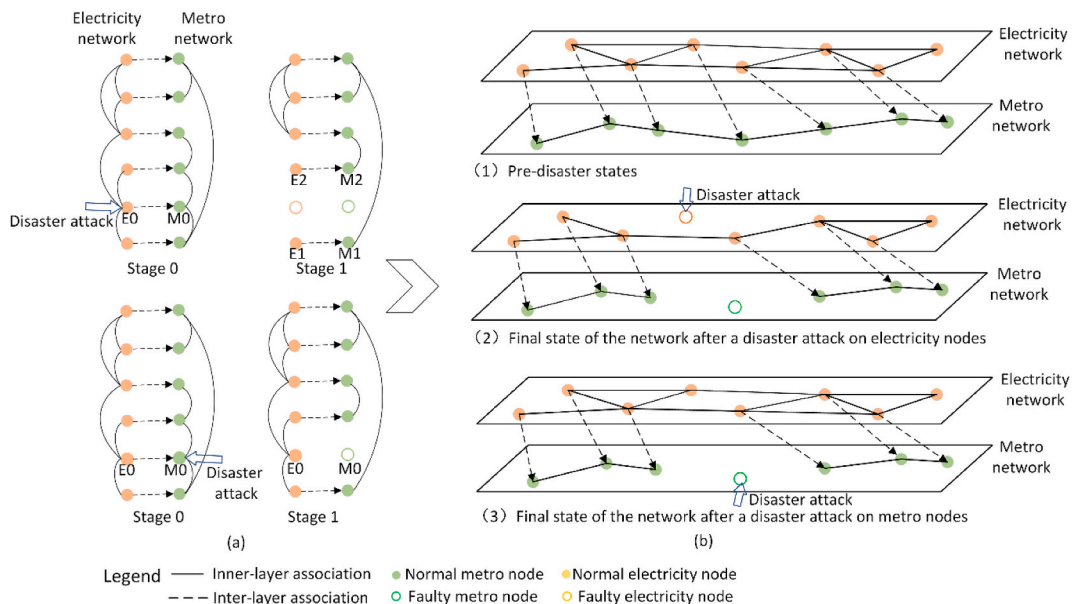

Fig. 5. The iterative process (a) and results (b) of cascading faults for power and subway nodes.

Conversely, if a subway station (M0) fails, only the edges of the metro network connected to it are removed, and this failure does not affect the normal use of the road section.

3.4. Disaster-damage model and risk assessment

3.4.1. Disaster chain risk

Since the disaster-causing factors considered in this paper include not only rainstorm hazards but also their secondary hazards, it is essential to assess the temporal risk of each node within the rainstorm disaster chain. Based on the disaster chain constructed above, the flood disaster risk resulting from heavy rainfall is simulated using the storm flood model in MIKE software, and the risk values for the other disaster nodes are calculated using the disaster chain risk assessment model.

In the stormwater model, the study area is divided into 200m × 200m spatial grids. Utilizing precipitation data published by the China Meteorological Administration (CMA), along with the elevation and land use characteristics of the study area, the spatial distribution of water accumulation following rainfall is simulated with MIKE21 to evaluate the risk level of flood hazards.

Regarding the risk assessment of other disaster nodes, most previous studies on disaster chain risk assessment have calculated risk levels as the product of disaster occurrence probability and potential loss [51–53]. This paper assesses the risk of disaster chain nodes by adapting the calculation model of disaster loss degree used in these studies, as follows.

$$S_{j\to i}(t) = \alpha_{j\to i}. \left[\left(\frac{1}{r}-1\right).\varepsilon_{j\to i}+1\right]P_{j\to i}.\beta^{t-t_{j\to i}}.S_j\left(t-t_{j\to i}\right)(i,j=1,2,3\ldots n) \tag{1}$$

$$t-t_{j\to i} < 0, \beta^{t-t_{j\to i}} = 0; \quad t-t_{j\to i} \geq 0, \beta^{t-t_{j\to i}} = 1 \tag{2}$$

where, $S_{j\to i}(t)$ represents the node loss degree; $\alpha_{j\to i}$ represents the relationship strength factor; r indicates the disaster intervention capability, which usually takes values between 0 and 9, with a higher value indicating a stronger government intervention power; $\varepsilon_{j\to i}$ equals to 1 or 0 indicates that there is or there is no government intervention between the two disaster nodes, respectively; $P_{j\to i}$ denotes the probability that the parent disaster event triggers the child disaster event; $\beta^{t-t_{j\to i}}$ denotes the delay coefficient, which belongs to the judgment function and is set in order to avoid the negative value of disaster loss degree when $t-t_{j\to i}$; t denotes the time of disaster evolution. The values of the node parameters need to be set according to the actual situation of the study area.

3.4.2. Impact of disasters

A disaster system is usually a complex system composed of disaster-causing factors, disaster-bearing environment, and disaster-bearing body. The above section describes the calculation method of the disaster loss degree of the parent disaster node in the disaster-causing factor leading to the child disaster node. The parameters of the equation involved in calculating the loss degree of the disaster-causing factor leading to the disaster-bearing body are somewhat like the calculation of the disaster loss degree, because both are calculating the damage of the nodes due to risk transmission in the complex system. Therefore, referring to the existing studies [53, 54], the equation for calculating the damage of disasters to infrastructure nodes is as follows:
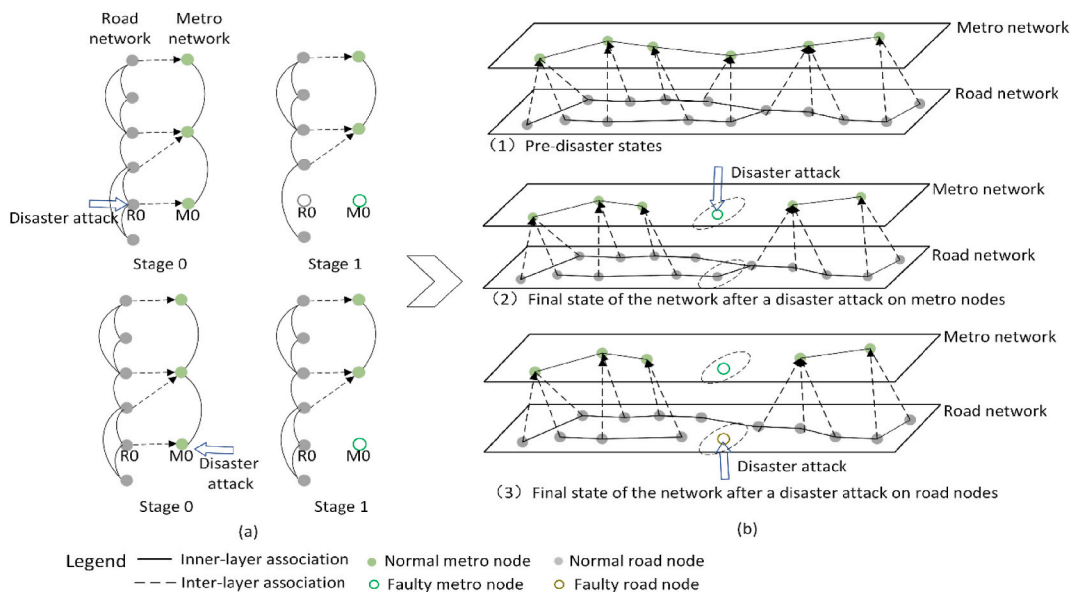

Fig. 6. The iterative process (a) and results (b) of cascading faults for subway and road section nodes.

$$X_i = \sum B_{ki} H_k(t)(t - t_{ki}) e^{-\beta t_{ki}/\tau_i} + \xi_i(t) \tag{3}$$

$$F_i = \begin{cases} 1, (X_i < \theta) \\ 0, (X_i \geq \theta) \end{cases} \tag{4}$$

Equation (3) represents the calculation of damage to infrastructure nodes caused by a hazard and its secondary effects. In Equation (3), X_i is the damage state of infrastructure node i; B_{ki} denotes the connection strength between the disaster-causing factor k and the infrastructure node I; H_k denotes the risk level of the disaster-causing factor k; t_{ki} and β are damping coefficients and time delay coefficients, which denote the time delay and loss spread delay of infrastructure damage caused by disaster-causing factor respectively; τ_i denotes the self-recovery capability of the infrastructure node; $\xi_i(t)$ denotes the random term. The results of X_i calculated through the above formulation are continuous numerical data rather than categorical data; thus, its outcomes are capable of reflecting the extent of damage to the infrastructure. θ represents the threshold, when the damaged state of the infrastructure node exceeds the threshold, it is defined as its function failure. The normal working state or failure of the infrastructure node is represented by F_i equal to 1 or 0, respectively. The specific values of the above parameters also need to be set according to the actual situation of the study area.

3.4.3. State of infrastructure nodes under the influence of the disaster chain effect

The risk level of the rainstorm disaster chain is calculated according to Equations (1) and (2), and the damage of the rainstorm disaster chain risk to infrastructure nodes and the final state of the nodes are calculated according to Equations (3) and (4). Fig. 7 shows the impact of the rainstorm disaster chain on infrastructure nodes. There are differences in the level of disaster risk at different locations in the study area, and so does the level of secondary disaster risk caused by storms. These differences do not only appear spatially but are also temporal. The aim of this paper is then to carry out a refined assessment of the risk of infrastructure nodes under the influence of subdivided disaster chains in different spaces and different times. As previously mentioned, the risk of heavy rainfall and its secondary disasters is obtained by dividing the study area into 200m×200m grids and calculating the disaster risk within each grid separately. Also, the calculation of the impact of disasters on infrastructure nodes using the disaster loss formula was also carried out separately within these small 200m×200m grids, thus achieving the purpose of calculating the level of infrastructure risk in a fine-grained manner from the micro-scale. In addition, the spatial location information of each infrastructure node is incorporated into the model. When the failed infrastructure nodes are output every 10 min in Python software, the location information of each node can be displayed, forming the spatial distribution map of failed nodes at multiple time points, and realizing the timed and location-specific infrastructure risk assessment.

4. Application

4.1. Case study

The refined risk assessment and theoretical model constructed in the previous section were validated against a heavy rainfall scenario that typified a meteorological disaster affecting Dongguan City in 2023. Dongguan, located in South-central Guangdong Province on the eastern coast of the Pearl River Estuary, serves as the central hub of the eastern Pearl River Delta and is one of China's key economic centers. Designated as a mega-city by the State Council of China, Dongguan enjoys a strategic geographic position, bordered by Guangzhou City to the northwest, Shenzhen City to the south, and Huizhou City to the northeast. Covering a total area of 2,542.67 square kilometers, Dongguan exhibits a high urbanization rate, significant urban infrastructure, and dense population.

However, the city faces considerable meteorological challenges. Dongguan is influenced year-round by monsoons, resulting in abundant precipitation and uneven rainfall distribution due to its location within the subtropical monsoon climate zone. The city is particularly susceptible to heavy rainfall and other adverse climatic conditions, including typhoons and monsoonal low pressure
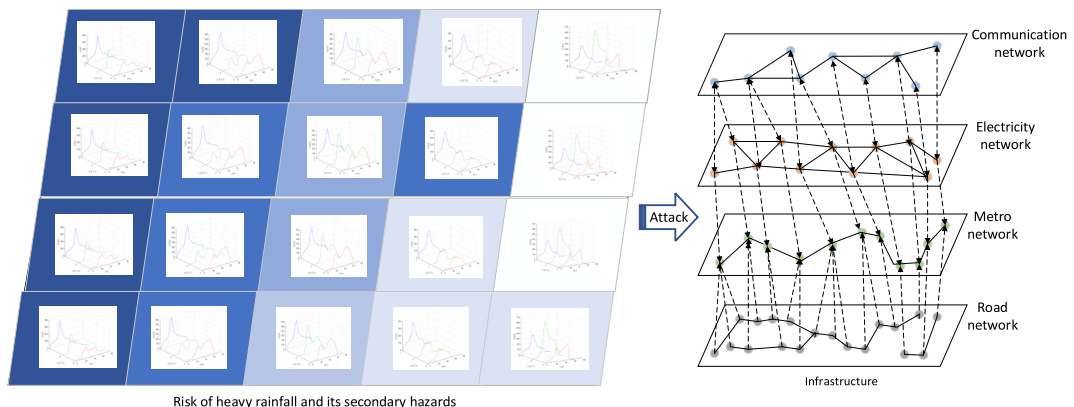

Fig. 7. Schematic diagram of the impact of a rainstorm disaster chain on infrastructure nodes.

systems. Consequently, the lives of citizens and the stability of their properties are constantly threatened by heavy rainfall hazards, which can cause waterlogged roads, flooding, power outages, and subsequent economic impacts. Given that rainstorms represent the meteorological disaster with the highest probability of occurrence and the most severe losses in Dongguan, the risk assessment theoretical model developed in this study focuses exclusively on scenarios where rainstorms are the primary disaster. The case study selected for validation also centers on scenarios in which rainstorms constitute the predominant meteorological disaster.

Numerous cities worldwide share characteristics similar to those of Dongguan, including Bangkok, Tokyo, and Seoul in Asia, and London, Paris, and Amsterdam in Europe, as well as New York, Toronto, and Mexico City in North America. These cities, influenced by high-density infrastructure and populations, are under constant threat from the frequent occurrence of heavy rainfall hazards [55,56]. Therefore, this study related to Dongguan could serve as a model and proof of concept. The developed framework can be utilized by local and national authorities to investigate the risks to infrastructure posed by heavy rainfall hazards, along with the consequent cascading effects on essential services.

According to the Dongguan Meteorological Bureau, from September 7th to 8th, 2023, the city experienced the most intense rainstorm in nearly 15 years. During this event, several towns and streets received over 250mm of rainfall, with Chang'an and Dalingshan towns recording 425.3mm and 415.2mm, respectively. This torrential rain resulted in flooding across multiple locations, with 86 waterlogged spots identified within the city, where water depths ranged from 0.2 to 1.5m. Traffic was severely disrupted on many road sections due to flooding, significantly affecting the daily lives and travel of local residents. Additionally, the heavy rainfall triggered secondary effects, including mudslides and collapses, posing serious threats to the safety of lives and property. For this study, the authors collected real-time datasets on this meteorological disaster and its resultant consequences over a total of 22h, from 9:00 p. m. on September 7th to 7:00 p.m. on September 8th, 2023. Consequently, this extreme meteorological disaster was employed to evaluate the performance of the theoretical model developed to analyze the risks associated with such scenarios.

4.2. Modeling setup

Typical rainstorm disaster cases that affected Dongguan City over the past decade (2014–2023) were collected from the official websites of the Dongguan Emergency Management Bureau (http://dgsafety.dg.gov.cn/gkmlpt/index), the Dongguan Meteorological Bureau (http://gd.cma.gov.cn/dgsqxj/mobile/), the Dongguan Natural Resources Bureau (http://nr.dg.gov.cn/gzhd/dczj/index.html), Baidu news pages (https://news.baidu.com/) and the China Knowledge Network (https://www.cnki.net/) using web crawlers.) using web crawlers. In total, 42 heavy rainfall events were utilized as the foundational text data for constructing the disaster chain effects in Dongguan City. The secondary effects associated with these rainstorms, as extracted from the text data, primarily included floods, collapses or landslides, road traffic accidents, electric power failures, communication disruptions, and subway incidents. Given that road traffic, electric power, communication, and subway systems are the primary infrastructure disaster-bearing entities considered in this study, the disaster-causing factors primarily focus on heavy rainfall and its resulting secondary effects, specifically "flooding" and "collapse or landslide." Based on the correlation relationships between the hazards identified in the text, a simple correlation network depicting heavy rainfall and its secondary effects is illustrated in Fig. 8.

4.3. Disaster chain risk assessment

Flood risk induced by rainstorm hazards was assessed by analyzing the spatial and temporal distribution of regional waterlogging volumes. First, it was essential to establish the rainfall amounts for each specific area involved. Second, hydrological and pipe-flow simulations were conducted from 9:00 p.m. on September 7, 2023, to 7:00 p.m. on September 8, 2023, resulting in a total of 66 simulations, with outputs exported at 20-min intervals. Finally, the potential risk of flooding was evaluated by analyzing the distribution of standing water in each area based on the simulation results.

Fig. 9 illustrates the distribution of standing water resulting from heavy rainfall at the 8th, 18th, and 27th time points selected from the 66 simulations. To accommodate space limitations, the depth of standing water caused by heavy rainfall was categorized into three levels: low, medium, and high, using clustering techniques. The median values of standing water in these three categories were chosen for the time points of 8, 18, and 27, as they effectively reflect overall conditions and provide an accurate representation of observed trends. The results indicate that flood risk varies across different times and locations.

The risk of collapses and mudslides in the disaster chain was calculated by the product of the degree of disaster loss and the
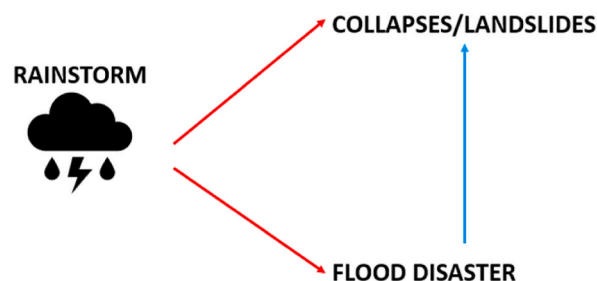

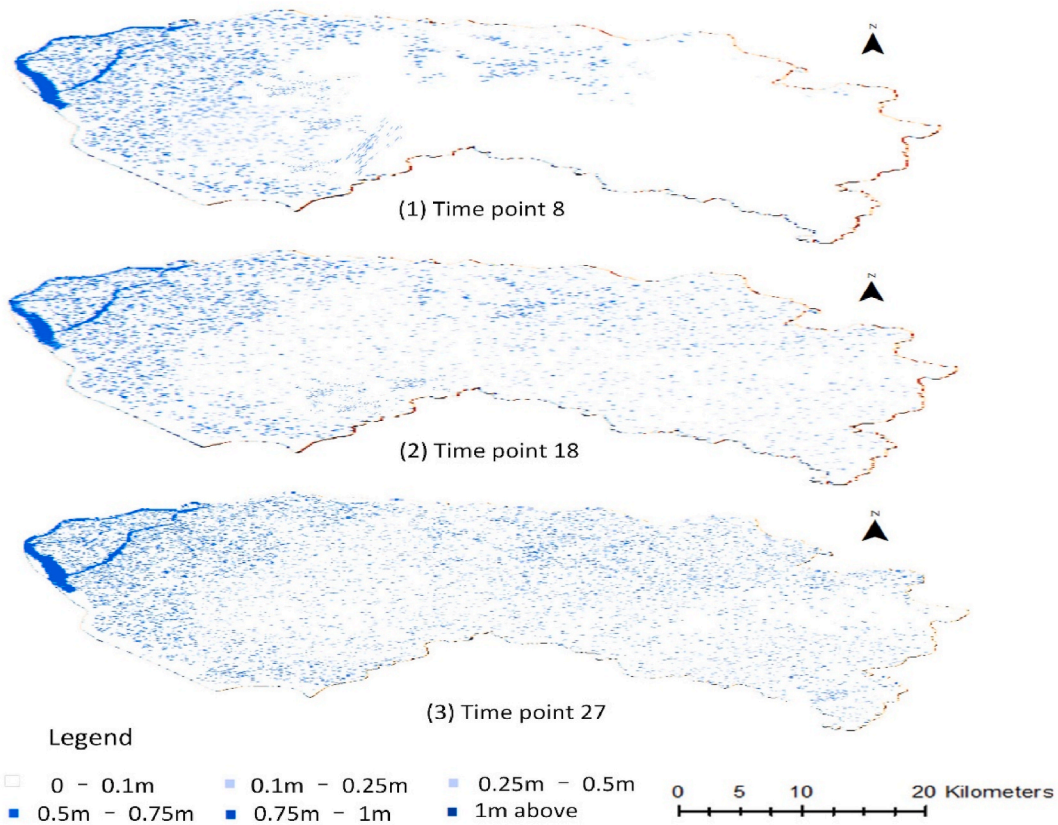**Fig. 8.** Secondary hazards induced by a rainstorm hazard.

Fig. 9. Distribution of standing water due to heavy rainfall within specific locations and times.

probability of occurrence of the disaster. By referring to previous studies and the actual situation of the study area, the parameter r (denoting the government intervention power as mentioned in Equation (1)) is set to 1.5 for both paths "heavy rainfall → collapse/landslide" and "flood → collapse/landslide" in Fig. 8. The delay coefficients are set to t $_{heavy\ rainfall\ \to\ flooding}$ = 6, t $_{heavy\ rainfall\ \to\ collapse/landslide}$ = 15, and t $_{flooding\ \to\ collapse/landslide}$ = 30 (larger values indicate longer event intervals between the occurrence of the parent hazard event and the occurrence of the child hazard event), with a total evolution time of 66. The average risk level of the collapse and mudslide nodes in the study area was calculated according to Equation (1), and the time-series risk distribution of the three hazard nodes is shown in Fig. 10. Considering that the levels of risk from heavy rainfall and its secondary hazards vary in different regions, the time-series evolution of the hazard risk was plotted in Fig. 10 using the average risk level of the whole region. The average risk level of collapse and mudslide nodes was classified using the interquartile method, and risk values in the third and fourth quartile intervals
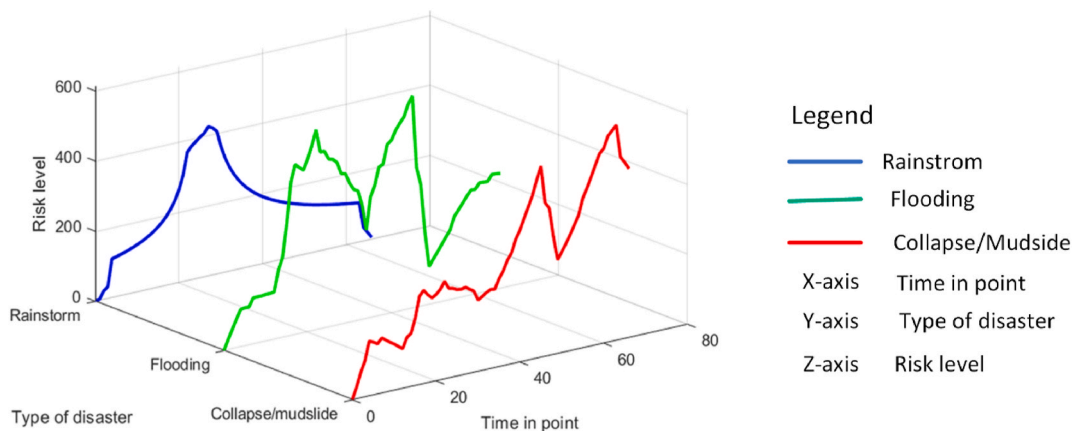

Fig. 10. Time-series evolution of the average risk level of heavy rainfall and its secondary hazards across the region studied.

were defined as high risk. The risk of infrastructure failure is higher in areas at high risk of collapse and mudslide.

4.4. Infrastructure cascade failure analysis

Fig. 11 presents the schematic diagram of the infrastructure cascade fault correlation network model for Dongguan, developed based on the previously described infrastructure cascade fault mechanism. The relationships within and between various infrastructure layers in Dongguan were partially constructed to reflect real-world conditions. Specifically, the connections between nodes within the road and metro layers are based on actual road lines and metro lines, respectively.

According to previous studies, the electricity network in China exhibits small-world characteristics [57], while the communication network is typically characterized as a scale-free network [58]. Utilizing the realistic spatial distribution of power plants, substations, charging stations, and power authorities in Dongguan, the model incorporates small-world network attributes (short average path lengths, high clustering coefficients, etc.) and scale-free network features (node heterogeneity, preferential attachment, etc.). The algorithms referenced in earlier studies ([22,25]; see Equation (5)) were employed to construct the electricity and communication networks of Dongguan.

For the interconnections between these networks, each electricity node is linked to the nearest communication node, each metro node is connected to the nearest electricity node, and each road node is associated with the nearest metro node. This approach results in the formation of a coupled system network encompassing electricity, communication, metro, and road infrastructures in Dongguan. The aforementioned steps were implemented through programming in Python software.

$$(\omega_i + \omega_j)h(d) \geq \theta; \quad h(d) = d^{-2} \tag{5}$$

where, ω_i and ω_j are the weights of nodes i and j, representing the status of the nodes within the network, and the higher values indicate a higher probability of connection with other nodes. For electricity nodes, the weights of substations and power plants are set to 5, and the weight of other power station are set to 1. For communication nodes, the weight of the power information dispatch centers is 5, and the weights of other information points are set to 1. $h(d)$ represents the probability of connection between two nodes at a distance d. In reality, it is generally that the farther apart two nodes are, the less likely they are to be connected. Therefore, $h(d)$ is set to the inverse square of d, with d being the geodesic distance. θ is a threshold, when the product of the weight and the probability h exceeds this threshold, it indicates that there is a high probability of a connection between the nodes. The thresholds for both the electricity and
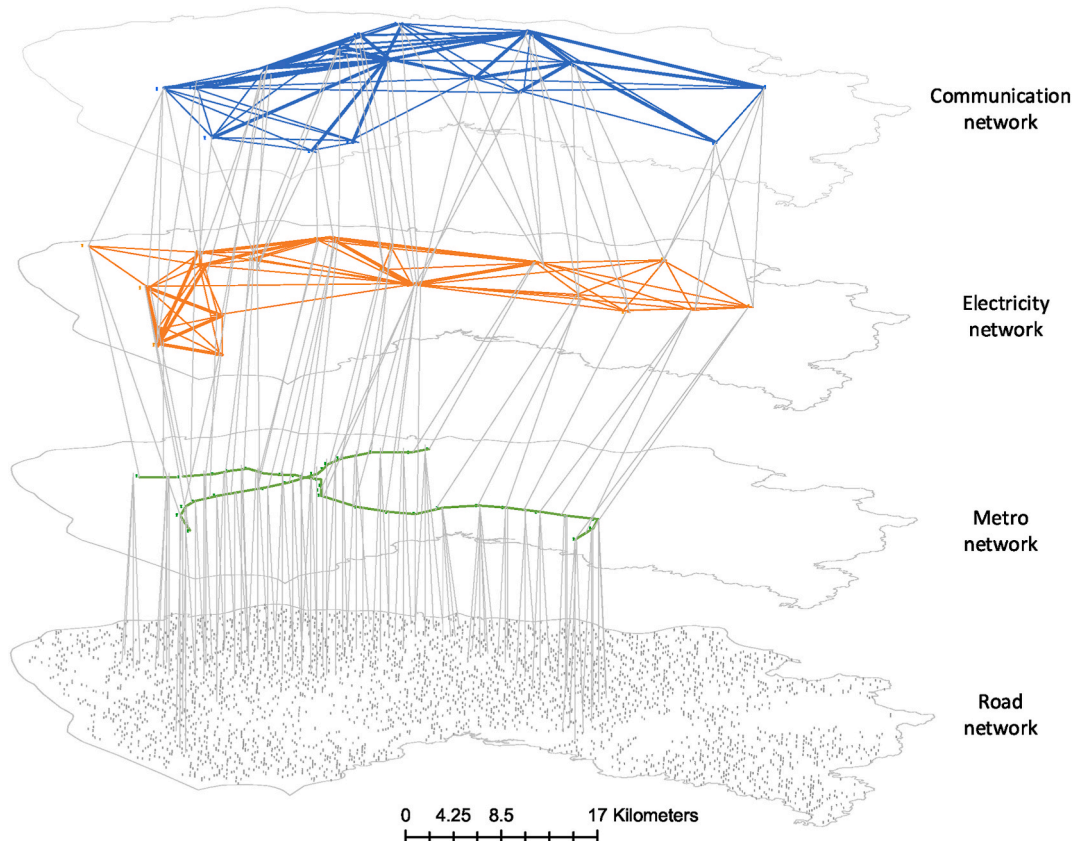

Fig. 11. Schematic diagram of the infrastructure association network.

communication layers are set to 0.05.

Due to the interdependence between communication nodes and power nodes, faults resulting from disaster impacts are assumed to be transmitted reciprocally between these nodes. In contrast, because of the unilateral dependency between power nodes and metro nodes, faults caused by disasters are only transmitted from power nodes to metro nodes. Similarly, a unary dependency exists between metro and road nodes. Specifically, failures in road infrastructure (including national highways, provincial highways, county highways, primary roads, secondary roads, tertiary roads, and quaternary roads, as previously mentioned) within a 100-m radius of the metro station can lead to metro failures due to reduced accessibility. Conversely, the transmission of failures from metro to road infrastructure is considered to be an extreme and rare occurrence and is, therefore, generally negligible.

5. Results and discussion

5.1. Results of spatio-temporal distribution for failed nodes

The risk level induced by each heavy rainfall event and its secondary hazards allows for the calculation of damage to infrastructure nodes, determining whether a node fails, using Equations (3) and (4) as previously described. In this study, thresholds were established at 0mm for subways and 300mm for roads, indicating that water accumulation exceeding these depths would result in the failure of the respective infrastructures. Any regional infrastructure nodes located within the high-risk zone for collapse or mudslides were classified as failed. The values of the remaining parameters are presented in Table 1.

The strength of association B_{ki} (Table 1 and Equation (3)) was derived from data on the 42 rainstorm events recorded in Dongguan City. A larger value of the restoration capability τ_i signifies a weaker inherent restoration capacity of the node itself. Given that regulators place significant emphasis on post-disaster infrastructure repair and allocate substantial resources for this purpose, resilience is considered low, and the differences in resilience and damping coefficients between pathways are minimal. Since infrastructure damage caused by collapse or mudslides typically occurs over a relatively brief time frame, the delay coefficient is set to 1, equating to a duration of 20 min; conversely, the delay coefficients for other pathways are comparatively longer.

Based on the cascading failure mechanisms among infrastructure nodes and the secondary effects induced by heavy rainfall, this study quantified the storm's impact on infrastructure nodes by assessing their status at various times and locations. This approach facilitated a timely and refined risk assessment for each infrastructure node.

Fig. 12 illustrates the number of failed infrastructure nodes over time. As anticipated, there was an initial surge in the number of nodes affected by heavy rainfall; however, the situation gradually stabilized, and nodes progressively returned to operational status. The peak failure of road nodes occurred at time point 19 (i.e., 15:00 on September 7), followed by a fluctuating decline, with two subsequent minor peaks at time points 47 (0:20 on September 8) and 62 (5:20 on September 8). Conversely, the peak failure of power nodes was recorded at time point 14 (i.e., 13:20 on September 7), with all power nodes returning to normal operation within 1h. This rapid recovery can be attributed to the small-world characteristics of the power network, which facilitates close connections between substations and multiple charging stations. The timely repair of key substations allowed for the swift restoration of power across extensive areas, resulting in the rapid recovery of over 500 electrical nodes within 1h.

In contrast, communication and metro nodes exhibited fewer failures, with no metro nodes experiencing failure throughout the entire event. The peak failure of communication nodes also occurred at time point 14, with all communication facilities returning to normal operation within 1h.

Fig. 13 illustrates the spatial distribution of failed infrastructure nodes at three selected time points (19, 48, and 64), specifically highlighting road failure nodes characterized by prolonged durations and a substantial number of failures. This selection was informed by the results presented in Fig. 12, where the time points corresponding to the three minor peaks in roadway failures were emphasized for display (i.e., time points 19, 48, and 64).

The results indicate that the failing roads did not exhibit significant aggregation characteristics during the early stages and were distributed across various regions of Dongguan. This scattering may be attributed to Dongguan's polycentric structure, which comprises 33 towns and streets. Each region contains low-lying areas susceptible to waterlogging and inadequate drainage, resulting in

Table 1
Coefficients utilized in the simulation model and their assigned values.

| Parameter/Path	Strength of association B_{ki}	Damping coefficient t_{ki}	Delay coefficient β	Resilience τ_i
Storm→Electricity	0.18	0.3	9	2
Storm→Communication	0.06	0.3	9	2
Storm→Metro	0.06	0.4	9	3
Storm→Road	0.41	0.4	9	3
Flooding→Electricity	0.41	0.3	15	2
Flooding→Communication	0.12	0.3	15	2
Flooding→Metro	0.59	0.4	1	3
Flooding→Road	0.71	0.4	6	3
Collapse/mudslide→Electricity	0.06	0.4	1	2
Collapse/mudslide→Communication	0.03	0.4	1	2
Collapse/mudslide→Metro	0	0.4	1	2
Collapse/mudslide→Road	0.18	0.4	1	3
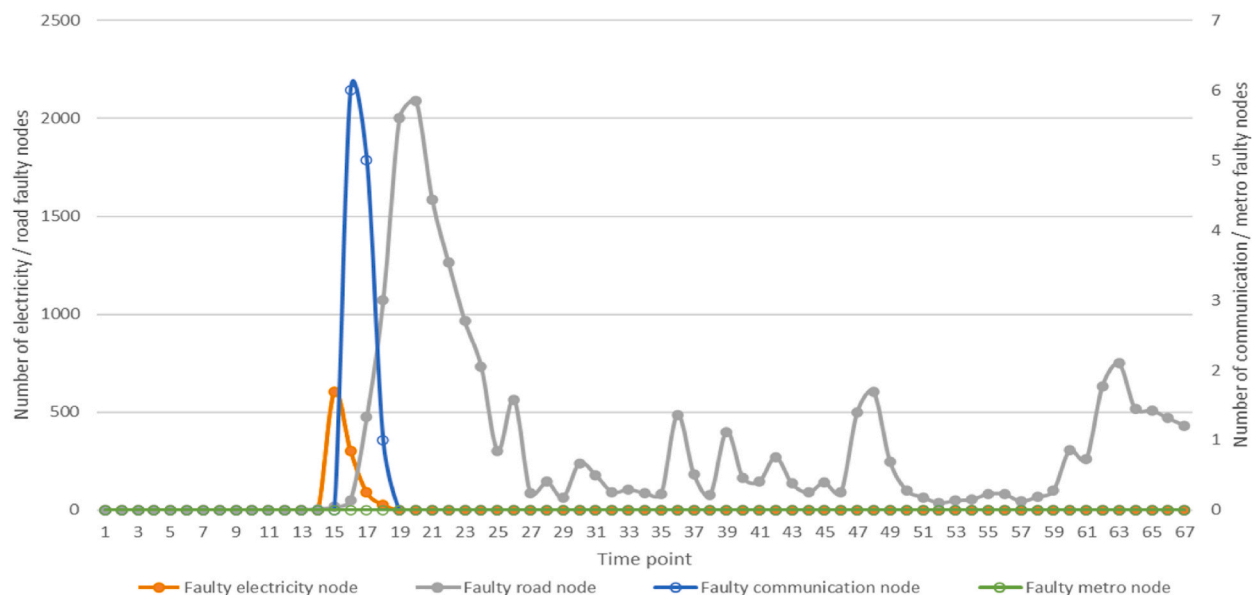
Fig. 12. Timing evolution of failed infrastructure nodes.

road failures following severe flooding. Over time, a noticeable increase in failed road nodes was observed in the southern townships compared to the northern townships. This trend likely reflects the progressive emergence of secondary effects induced by heavy rainfall.

5.2. Results validation

To evaluate the accuracy of the model results, this study conducted a refined risk assessment of infrastructure nodes following the release of rainfall forecast data for September 7th-8th, 2023, provided by the Dongguan Meteorological Bureau. This assessment yielded the spatial and temporal distribution of infrastructure nodes that were predicted to have failed as a consequence of the rainstorm.

Eighteen failure nodes identified by the model simulation results were selected for field investigation on September 7th-8th, 2023. The findings from these field observations were then compared with the model simulation outcomes to assess the model's accuracy. To determine the observation times, three minor peaks in the number of failed road nodes corresponding to time points 19, 48, and 64 were selected for the field investigation.

For the selection of the 18 observation sites, time point 64 was used as an example. The Probability Proportional to Size (PPS) sampling method was employed for sample selection (see Fig. 14). In this method, the probability of selecting a specific failed node within a town was proportional to the number of failed nodes in that town relative to the total number of failed nodes. Once the number of failed nodes designated for field investigation in each town was determined, specific nodes corresponding to these locations were selected through random sampling for field investigation. The same methodology was applied to select survey locations for the other two time points, namely time points 19 and 48. Ultimately, a total of 54 observations were conducted across the three time points.

Table 2 presents a comparison between the simulation results and real-world observations. Overall, 38 out of 54 simulated results were accurate, yielding an accuracy rate of 70.4%. The simulation results at time point 19 exhibited the highest accuracy, at 77.8%, while those at time points 48 and 64 demonstrated lower accuracy rates of 66.7%. This discrepancy may arise from the fact that the simulation results at time point 19 primarily reflect the immediate impacts of heavy rainfall disasters on infrastructure. In contrast, the secondary effects of heavy rainfall gradually manifest at time points 48 and 64. The dual influence of errors in simulating secondary disaster risks and errors in modeling the initial disaster impacts contribute to the overall decline in simulation accuracy.

In summary, the theoretical model developed in this paper can adequately represent the impacts of heavy rainfall and its secondary hazards on infrastructure, achieving approximately 70% accuracy. However, it does not fully capture all aspects of the real-world situation. Nevertheless, we believe that the model's accuracy can be enhanced through the incorporation of additional field data.

The enhancement of risk assessment accuracy through the use of realistic or field data can be attributed to three key aspects: First, by extracting the types and probabilities of secondary disasters induced by heavy rainfall based on more detailed and accurate real-case scenarios, the construction of the rainstorm disaster chain and the subsequent calculations of risk for secondary disasters can be improved. Second, establishing real connections between infrastructures based on realistic or field data can enhance the accuracy of cascading fault conduction calculations. Third, during the model testing phase, continuously refining the coefficients involved in the theoretical disaster loss model (e.g., delay coefficients, disaster intervention capability coefficients) based on field data can increase
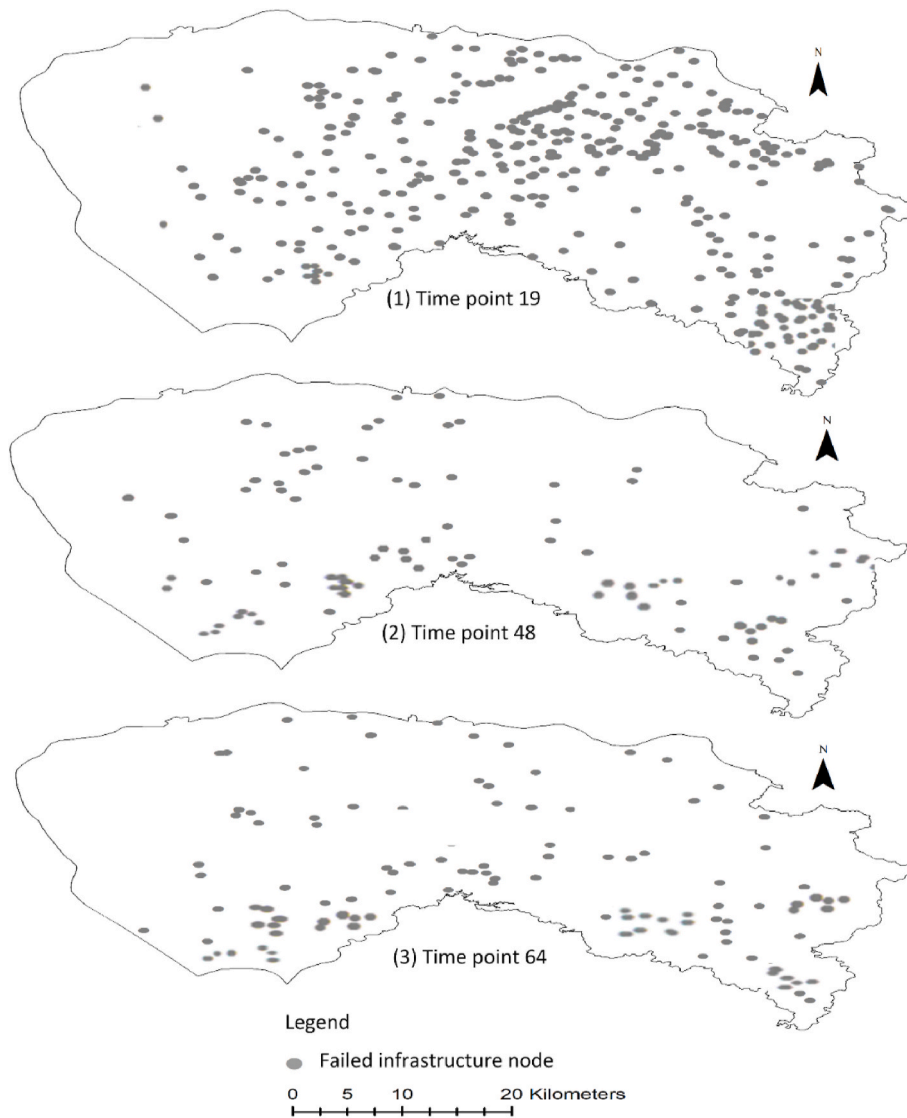
Fig. 13. Spatial distribution of failure nodes.

the accuracy of disaster loss assessments.

Additionally, other approaches may further enhance the accuracy of the risk assessment model. For instance, employing advanced simulation techniques, such as intelligent agent models or multi-agent systems, can provide a meticulous simulation of the behaviors and responses of infrastructure systems and their interactions following a hazard shock [59–61]. Alternatively, leveraging machine learning and artificial intelligence techniques to identify patterns and trends within large datasets can optimize the predictive power and accuracy of the risk assessment model [62–64]. However, these methodologies require validation through future research.

6. Conclusion

The refined assessment of risks induced by multiple hazards at specific times and locations has not been thoroughly investigated to date. This paper presents a methodology for assessing the risk of infrastructure nodes at various times and locations following the impact of heavy rainfall and its secondary hazards. This approach distinguishes itself from existing studies that focus either on the risk level of a single hazard or on a macro-system analysis. The developed model evaluates the initial impact of multiple hazards, identifies correlations between infrastructure nodes, and examines cascading failure effects among different nodes. The accuracy and effectiveness of the methods presented in this manuscript were validated against a 15-year heavy rainfall disaster that affected Dongguan City, with results indicating that the theoretical methods for refining infrastructure risk assessments under the influence of the rainstorm disaster chain can replicate real-life scenarios with approximately 70% accuracy.

Although the refined risk assessment model offered in this manuscript provides a significant reference for disaster risk prevention
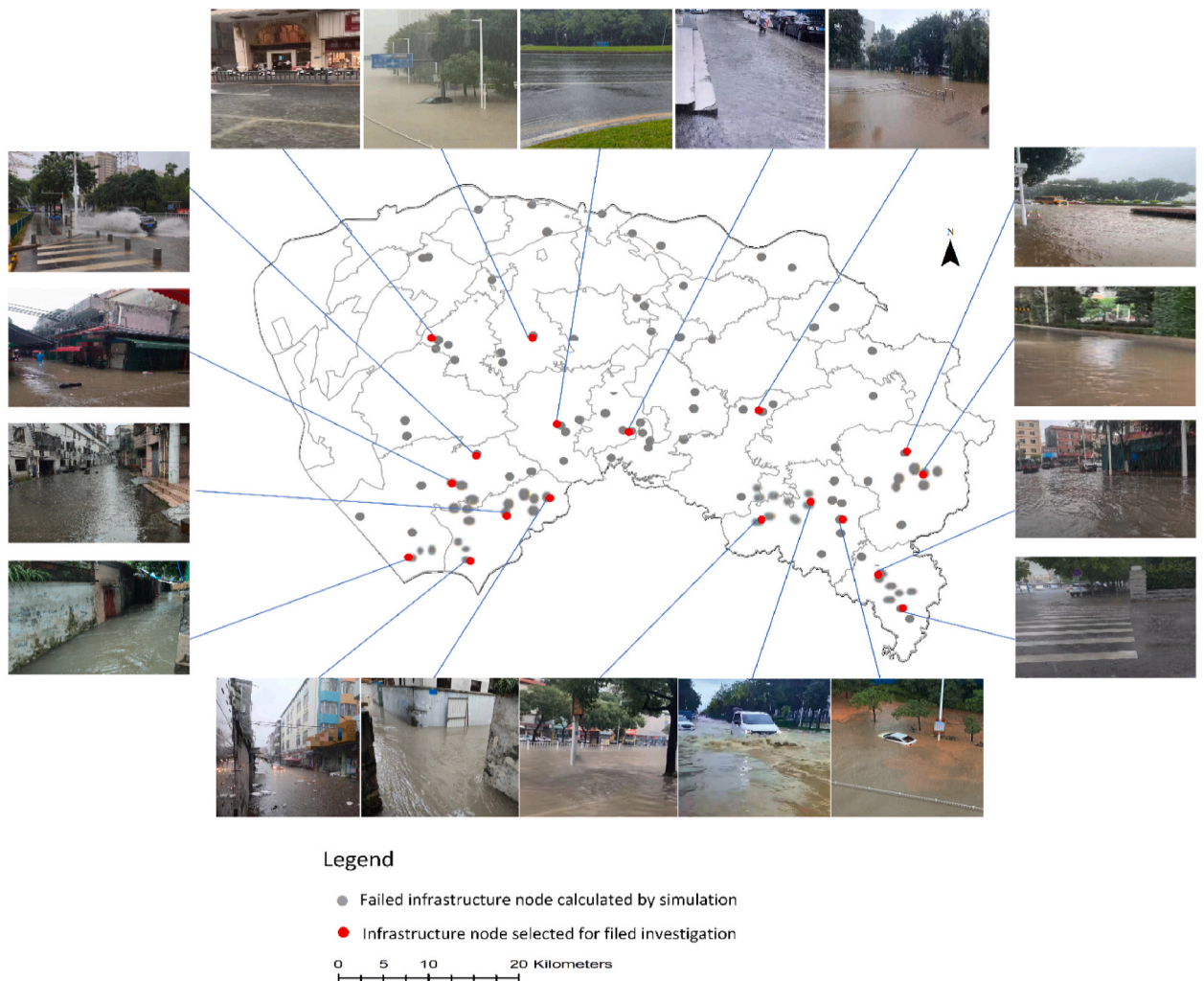
Fig. 14. Selection of sites for field investigation at time point 64. All the images in the figure were taken by the authors during the filed investigation.

and response at specific times and locations, several aspects require further enhancement. For instance, many parameters utilized in this study were derived from real datasets associated with the study area as well as empirical values from existing literature when real data were difficult or impossible to obtain. The reliance on this secondary data may have introduced minor inaccuracies and discrepancies, which could be mitigated with improved data availability. Thus, conducting a more in-depth analysis of the background and rationale for each parameter setting, combined with regional differentiation in each case study, is recommended to enhance the model's accuracy.

Furthermore, the disaster-causing factors examined in this paper are limited to heavy rainfall and its secondary hazards, such as flooding and mudslides. The infrastructures considered include only electricity, communication, and transportation (specifically subway and road systems). Expanding the scope to incorporate additional hazard types or infrastructure functions could increase model complexity and impact results, necessitating further investigation. Given the variety of meteorological hazard scenarios that cities worldwide may face, including rainstorms, typhoons, and storm surges, the refined infrastructure risk assessment methodology constructed in this study can be applied to different hazard scenarios. To do so, it is essential to update the primary hazards, their secondary effects, and the impact mechanisms on infrastructure, along with selecting realistic hazard scenarios for model verification. Due to space limitations and the unique complexities associated with each meteorological hazard scenario, updates and verifications for other meteorological hazards should be pursued in future research.

Additionally, the analysis of cascading fault conduction in this study may not fully capture the complexities of real-world operations. For instance, subway stations may utilize dedicated power lines with redundancies that could influence the cascading fault conduction relationships between power failure nodes and subway station nodes. To improve the accuracy and applicability of cascading fault analysis, future research should further refine the operational model of metro lines and explore empirical data regarding power system redundancy and cascading fault conduction, thereby enhancing the model's value in real-world disaster

Table 2
Comparison of simulation results against field observations results.

Observation points	Time 19		Time 48		Time 64	
	Simulation results	Field observations results	Simulation results	Field observations results	Simulation results	Field observations results
Node 1	Failed	Failed	Failed	Failed	Failed	Normalized
Node 2	Failed	Failed	Failed	Failed	Failed	Failed
Node 3	Failed	Normalized	Failed	Failed	Failed	Failed
Node 4	Failed	Failed	Failed	Failed	Failed	Normalized
Node 5	Failed	Failed	Failed	Normalized	Failed	Failed
Node 6	Failed	Failed	Failed	Failed	Failed	Failed
Node 7	Failed	Normalized	Failed	Failed	Failed	Normalized
Node 8	Failed	Normalized	Failed	Failed	Failed	Normalized
Node 9	Failed	Failed	Failed	Normalized	Failed	Failed
Node 10	Failed	Failed	Failed	Normalized	Failed	Failed
Node 11	Failed	Failed	Failed	Normalized	Failed	Normalized
Node 12	Failed	Failed	Failed	Failed	Failed	Failed
Node 13	Failed	Failed	Failed	Failed	Failed	Failed
Node 14	Failed	Failed	Failed	Normalized	Failed	Normalized
Node 16	Failed	Failed	Failed	Normalized	Failed	Failed
Node 17	Failed	Normalized	Failed	Failed	Failed	Failed
Node 18	Failed	Failed	Failed	Failed	Failed	Failed
Accuracy rate	77.8%		66.7%		66.7%	
	Average accuracy: 70.4%					

management applications.

Nonetheless, the authors firmly believe that this study provides a foundational basis for implementing new rescue policies during heavy rain hazards. By identifying locations under significant threat, local and national authorities can allocate targeted resources and support where it is most needed. Furthermore, managers can integrate cutting-edge technological approaches—such as big data, smart algorithms, and digital twins—to present infrastructure risk assessment results and alert the public [65–67]. For example, residents could scan a QR code linked to a specific infrastructure to obtain real-time forecasts of its risk level. Alternatively, managers could combine the locations of residents' mobile devices with big data on travel patterns to identify users potentially associated with compromised infrastructure nodes. Consequently, text alerts could be sent to these residents, informing them of the time and location of infrastructure nodes likely to fail in the near future, prompting them to take preemptive and preparatory measures to reduce their exposure and vulnerability, thereby mitigating potential losses caused by disasters.

CRediT authorship contribution statement

Fan Li: Writing – review & editing, Writing – original draft, Visualization, Validation, Software, Methodology, Investigation, Formal analysis, Data curation, Conceptualization. **Yan Li:** Writing – review & editing, Writing – original draft, Validation, Investigation, Formal analysis, Data curation. **Matteo Rubinato:** Writing – review & editing, Writing – original draft, Supervision, Methodology, Investigation, Data curation. **Yu Zheng:** Writing – review & editing, Visualization, Software, Methodology, Investigation, Data curation. **Tao Zhou:** Writing – review & editing, Supervision, Resources, Project administration, Methodology.

Declaration of competing interest

The authors declare that they have no known competing financial interests or personal relationships that could have appeared to influence the work reported in this paper.

Acknowledgements

Data availability

Data will be made available on request.

References

[1] C. Lashford, M. Rubinato, y. Cai, J. Hou, S. Albofathi, S. Coupe, S. Charlesworth, S. Tait, SuDS & sponge cities: a comparative analysis of the implementation of pluvial flood management in the UK and China, Sustainability 11 (1) (2019) 213, https://doi.org/10.3390/su11010213.

[2] M. Rubinato, A. Nichols, Y. Peng, Y. Zhang, C. Lashford, Y. Cai, P. Lin, S. Tait, Urban and river flooding: comparison of flood risk management approaches in the UK and China and an assessment of future knowledge needs, Water Sci. Eng. 12 (4) (2019) 274–283, https://doi.org/10.1016/j.wse.2019.12.004.

[3] Y. Guan, F. Zheng, P. Zhang, C. Qin, Spatial and temporal changes of meteorological disasters in China during 1950–2013, Nat. Hazards 752607–2623 (2015).

[4] Ministry of Emergency Management, 2021 Global Natural Disaster Assessment Report, 2022.

[5] H. Tabari, Climate change impact on flood and extreme precipitation increases with water availability, Sci. Rep. 10 (1) (2020) 13768.

[6] United Nations Office for Disaster Risk Reduction, Why are disasters not natural?, Available online: https://www.undrr.org/our-impact/campaigns/no-natural-disasters, 2024. (Accessed 5 September 2024).

[7] D. Mcclean, Sendai Framework 6th Anniversary: time to recognize there is no such thing as a natural disaster - we're doing it to ourselves, Available online: https://www.undrr.org/news/sendai-framework-6th-anniversary-time-recognize-there-no-such-thing-natural-disaster-were, 2021. (Accessed 5 September 2024).

[8] K. Chmutina, J. von Meding, L. Bosher, Language matters: dangers of the "natural disaster" misnomer. Global Assessment Report on Disaster Risk Reduction, 2019.

[9] P. Gireesh Kumar, V. Tejaswini, P. Kesava Rao, G. Jaya Shankar, Disaster mitigation and its strategies in a global context - a state of the art, Mater. Today: Proc. 456488–6492 (2021).

[10] H. Xu, Y. Li, Y. Tan, N. Deng, A scientometric review of urban disaster resilience research, Int. J. Environ. Res. Publ. Health 18 (7) (2021) 3677.

[11] A.L. Ramanathan, C. Sabarathinam, M.P. Jonathan, M.V. Prasanna, P. Kumar, F.M. Arriola, Environmental Resilience and Transformation in Times of COVID-19: Climate Change Effects on Environmental Functionality, Elsevier, 2021.

[12] S.R. Rajan, Risk, Disaster, and Vulnerability: an Essay on Humanity and Environmental Catastrophe, Univ of California Press, 2023.

[13] X. Zhai, Q. Ji, F. Wu, Measuring climate risks and impacts, in: Climate Finance: Supporting a Sustainable Energy Transition, Springer, 2024, pp. 137–188.

[14] R. Berariu, C. Fikar, M. Gronalt, P. Hirsch, Understanding the impact of cascade effects of natural disasters on disaster relief operations, Int. J. Disaster Risk Reduc. (2015) 12350–12356.

[15] A. Fekete, Critical infrastructure and flood resilience: cascading effects beyond water, Water 61370 (2019).

[16] F. Yu, X. Li, Improving emergency response to cascading disasters: applying case-based reasoning towards urban critical infrastructure, Int. J. Disaster Risk Reduc. (2018) 30244–30256.

[17] C. Zhu, J. Wu, M. Liu, J. Luan, T. Li, K. Hu, Cyber-physical resilience modelling and assessment of urban roadway system interrupted by rainfall, Reliab. Eng. Syst. Saf. 204107095 (2020).

[18] L. Jiao, Y. Zhu, X. Huo, Y. Wu, Y. Zhang, Resilience assessment of metro stations against rainstorm disaster based on cloud model: a case study in Chongqing, China, Nat. Hazards 116 (2) (2023) 2311–2337.

[19] S. Gong, Y. Ye, X. Gao, L. Chen, T. Wang, Empirical patterns of interdependencies among critical infrastructures in cascading disasters: evidence from a comprehensive multi-case analysis, Int. J. Disaster Risk Reduc. 95103862 (2023).

[20] H. Tang, J. Zheng, M. Li, Z. Shao, L. Li, Gauging the evolution of operational risks for urban rail transit systems under rainstorm disasters, Water 15 (15) (2023) 2811.

[21] J. Kong, S.P. Simonovic, C. Zhang, Resilience assessment of interdependent infrastructure systems: a case study based on different response strategies, Sustainability 11 (23) (2019) 6552.

[22] C. Hsu, M. Teng, S. Ke, A comprehensive method for seismic impact chain assessment of urban lifeline infrastructure: a case study of Taipei area, Taiwan, KSCE J. Civ. Eng. 25 (10) (2021) 3650–3661.

[23] W. Wang, S. Yang, F. Hu, H.E. Stanley, S. He, M. Shi, An approach for cascading effects within critical infrastructure systems, Phys. A Stat. Mech. Appl. 510164–177 (2018).

[24] Z. Li, W. Yan, Service flow changes in multilayer networks: a framework for measuring urban disaster resilience based on availability to critical facilities, Landsc. Urban Plann. 244104996 (2024).

[25] Y. Zhang, N. Yang, U. Lall, Modeling and simulation of the vulnerability of interdependent power-water infrastructure networks to cascading failures, J. Syst. Sci. Syst. Eng. (2016) 25102–25118.

[26] S. Lee, M. Choi, H. Lee, M. Park, Bayesian network-based seismic damage estimation for power and potable water supply systems, Reliab. Eng. Syst. Saf. 197106796 (2020).

[27] A. Fekete, Critical infrastructure cascading effects. Disaster resilience assessment for floods affecting city of Cologne and Rhein-Erft-Kreis, J. Flood Risk Manag. 13 (2) (2020) e312600.

[28] X. He, E.J. Cha, Modeling the damage and recovery of interdependent critical infrastructure systems from natural hazards, Reliab. Eng. Syst. Saf. 177162–175 (2018).

[29] Z. Gong, Y. Wang, G. Wei, L. Li, W. Guo, Cascading disasters risk modeling based on linear uncertainty distributions, Int. J. Disaster Risk Reduc. 43101385 (2020).

[30] A. Suppasri, E. Maly, M. Kitamura, G. Pescaroli, D. Alexander, F. Imamura, Cascading disasters triggered by tsunami hazards: a perspective for critical infrastructure resilience and disaster risk reduction, Int. J. Disaster Risk Reduc. 66102597 (2021).

[31] N. Goldbeck, P. Angeloudis, W.Y. Ochieng, Resilience assessment for interdependent urban infrastructure systems using dynamic network flow models, Reliab. Eng. Syst. Saf. 18862–79 (2019).

[32] C.Y. Lam, T. Shimizu, A network analytical framework to analyze infrastructure damage based on earthquake cascades: a study of earthquake cases in Japan, Int. J. Disaster Risk Reduc. 54102025 (2021).

[33] T.J. Huggins, F. E, K. Chen, W. Gong, L. Yang, Infrastructural aspects of rain-related cascading disasters: a systematic literature review, Int. J. Environ. Res. Publ. Health 17 (14) (2020) 5175.

[34] L. Lu, X. Wang, Y. Ouyang, J. Roningen, N. Myers, G. Calfas, Vulnerability of interdependent urban infrastructure networks: equilibrium after failure propagation and cascading impacts, Comput. Aided Civ. Infrastruct. Eng. 33 (4) (2018) 300–315.

[35] R. Zimmerman, Q. Zhu, C. Dimitri, A network framework for dynamic models of urban food, energy and water systems (FEWS), Environ. Prog. Sustain. Energy 37 (1) (2018) 122–131.

[36] Q. Cheng, A new mathematical framework and spatial decision support system for modeling cascade interdependency of critical infrastructure during geo-disasters, J. Earth Sci. (2017) 28131–28146.

[37] J. Beyza, E. Garcia-Paricio, J.M. Yusta, Applying complex network theory to the vulnerability assessment of interdependent energy infrastructures, Energies 12 (3) (2019) 421.

[38] P. Singh, V.S.P. Sinha, A. Vijhani, N. Pahuja, Vulnerability assessment of urban road network from urban flood, Int. J. Disaster Risk Reduc. (2018) 28237–28250.

[39] M. Bao, Y. Ding, C. Shao, Y. Yang, P. Wang, Nodal reliability evaluation of interdependent gas and power systems considering cascading effects, IEEE Trans. Smart Grid 11 (5) (2020) 4090–4104.

[40] R.A. Loggins, W.A. Wallace, Rapid assessment of hurricane damage and disruption to interdependent civil infrastructure systems, J. Infrastruct. Syst. 21 (4) (2015) 04015005.

[41] R. Bali, Disaster management cycle, Asian J. Geogr. Res. 7 (1) (2024) 85–93.

[42] D.F. Shmueli, C.P. Ozawa, S. Kaufman, Collaborative planning principles for disaster preparedness, Int. J. Disaster Risk Reduc. 52101981 (2021).

[43] T. Konami, H. Koga, A. Kawatsura, Role of pre-disaster discussions on preparedness on consensus-making of integrated flood management (IFM) after a flood disaster, based on a case in the Abukuma River Basin, Fukushima, Japan, Int. J. Disaster Risk Reduc. 53102012 (2021).

[44] Q. Wang, J. Hou, Hazard assessment of rainstorm-geohazard disaster chain based on multiple scenarios, Nat. Hazards 118 (1) (2023) 589–610.

[45] L. Ye, Y. Zhou, Y. Zhou, B. Niu, Instance analysis of rainstorm floods chain and chain-cutting disaster mitigation building, J. Catastrophol 33 (14) (2018) 65–70.

[46] F. Wang, Z. Xie, H. Liu, Z. Pei, D. Liu, Multiobjective emergency resource allocation under the natural disaster chain with path planning, Int. J. Environ. Res. Publ. Health 187876 (2022).

[47] H. Dui, K. Liu, S. Wu, Cascading failures and resilience optimization of hospital infrastructure systems against the COVID-19, Comput. Ind. Eng. 179109158 (2023).

[48] A. Smolyak, O. Levy, I. Vodenska, S. Buldyrev, S. Havlin, Mitigation of cascading failures in complex networks, Sci. Rep. 10 (1) (2020) 16124.

[49] A. Ghasemi, H. de Meer, Robustness of interdependent power grid and communication networks to cascading failures, IEEE Trans. Netw. Sci. Eng. 10 (4) (2023) 1919–1930.

[50] S.V. Buldyrev, R. Parshani, G. Paul, H.E. Stanley, S. Havlin, Catastrophic cascade of failures in interdependent networks, Nature 464 (7291) (2010) 1025–1028.

[51] D. Kirschbaum, C.S. Watson, D.R. Rounce, D.H. Shugar, J.S. Kargel, U.K. Haritashya, P. Amatya, D. Shean, E.R. Anderson, M. Jo, The state of remote sensing capabilities of cascading hazards over High Mountain Asia, Front. Earth Sci. 7197 (2019).

[52] N. Chen, L. Chen, Y. Ma, A. Chen, Regional disaster risk assessment of China based on self-organizing map: clustering, visualization and ranking, Int. J. Disaster Risk Reduc. (2019) 33196–33206.

[53] D. Munasinghe, T. Fernando, K. Keraminiyage, A. Karunawardena, A review of the disaster risk assessment perspectives, in: Progress in Landslide Research and Technology, Springer Nature, Switzerland, Cham, 2023, pp. 323–340.

[54] H. Guo, X. He, X. Lv, Y. Wu, Risk analysis of rainstorm-urban lifeline system disaster chain based on the PageRank-risk matrix and complex network, Nat. Hazards 120 (2024) 10583–10606.

[55] P. Hall, Planning for the Mega-City: a New Eastern Asian Urban Form? Routledge, 2019, pp. 3–36.

[56] J. Brotchie, P. Newton, P. Hall, J. Dickey, East West Perspectives on 21st Century Urban Development: Sustainable Eastern and Western Cities in the New Millennium, Routledge, 2019.

[57] Y. Nie, G. Zhang, H. Duan, An interconnected panorama of future cross-regional power grid: a complex network approach, Resour. Pol. 67101692 (2020).

[58] Z. Min, W. Muqing, Q. Lilin, A. Quanbiao, L. Sixu, Evaluation of cross-layer network vulnerability of power communication network based on multi-dimensional and multi-layer node importance analysis, IEEE Access (2021) 1067181–1067197.

[59] L. Zhuo, D. Han, Agent-based modelling and flood risk management: a compendious literature review, J. Hydrol. 591125600 (2020).

[60] A. Anshuka, F.F. van Ogtrop, D. Sanderson, S.Z. Leao, A systematic review of agent-based model for flood risk management and assessment using the ODD protocol, Nat. Hazards 112 (3) (2022) 2739–2771.

[61] R. Wen, S. Li, A review of the use of geosocial media data in agent-based models for studying urban systems, Big Earth Data 5 (1) (2021) 5–23.

[62] S. Ghaffarian, F.R. Taghikhah, H.R. Maier, Explainable artificial intelligence in disaster risk management: achievements and prospective futures, Int. J. Disaster Risk Reduc. 98104123 (2023).

[63] P.M. Labis, Machine learning for disaster risk reduction-review and research directions, Sciences (2024).

[64] A.S. Albahri, Y.L. Khaleel, M.A. Habeeb, R.D. Ismael, Q.A. Hameed, M. Deveci, R.Z. Homod, O.S. Albahri, A.H. Alamoodi, L. Alzubaidi, A systematic review of trustworthy artificial intelligence applications in natural disasters, Comput. Electr. Eng. 118109409 (2024).

[65] S.M. Khan, I. Shafi, W.H. Butt, I.D.L.T. Diez, M.A.L. Flores, J.C. Galán, I. Ashraf, A systematic review of disaster management systems: approaches, challenges, and future directions, Land 12 (8) (2023) 1514.

[66] H.S. Munawar, A.W.A. Hammad, S.T. Waller, A review on flood management technologies related to image processing and machine learning, Autom. ConStruct. 132103916 (2021).

[67] F. Yuan, C. Fan, H. Farahmand, Smart flood resilience: harnessing community-scale big data for predictive flood risk monitoring, rapid impact assessment, and situational awareness, Environ. Res.: Infrastruct. Sustain. 2 (2) (2022) 025006.